Cation Mediation of Radical Transfer between Trp48 and Tyr356 during O_2 Activation by Protein R2 of *Escherichia coli* Ribonucleotide Reductase: Relevance to R1−R2 Radical Transfer in Nucleotide Reduction?†

Lana Saleh and J. Martin Bollinger, Jr.*

Department of Biochemistry and Molecular Biology and Department of Chemistry, The Pennsylvania State University, University Park, Pennsylvania 16802

Received February 15, 2006; Revised Manuscript Received May 21, 2006

ABSTRACT: A tryptophan 48 cation radical ($W48^{+\bullet}$) forms concomitantly with the Fe_2(III/IV) cluster, **X**, during activation of oxygen for tyrosyl radical (Y122•) production in the R2 subunit of class I ribonucleotide reductase (RNR) from *Escherichia coli*. $W48^{+\bullet}$ is also likely to be an intermediate in the long-range radical transfer between R2 and its partner subunit, R1, during nucleotide reduction by the RNR holoenzyme. The kinetics of decay of $W48^{+\bullet}$ and formation of tyrosyl radicals during O_2 activation (in the absence of R1) in wild-type (wt) R2 and in variants with either Y122, Y356 (the residue thought to propagate the radical from $W48^{+\bullet}$ into R1 during turnover), or both replaced by phenylalanine (F) have revealed that the presence of divalent cations at concentrations similar to the [Mg^{2+}] employed in the standard RNR assay (15 mM) mediates a rapid radical-transfer equilibrium between W48 and Y356. Cation-mediated propagation of the radical from W48 to Y356 gives rise to a fast phase of Y• production that is essentially coincident with $W48^{+\bullet}$ formation and creates an efficient pathway for decay of $W48^{+\bullet}$. Possible mechanisms of this cation mediation and its potential relevance to intersubunit radical transfer during nucleotide reduction are considered.

Ribonucleotide reductases (RNRs)[1] catalyze conversion of ribonucleoside di- or triphosphates to the corresponding 2′-deoxyribonucleotides (*1*−*4*). The reaction proceeds via a free-radical mechanism that is initiated by abstraction of the 3′-hydrogen of the substrate (*5*−*7*) by a protein radical (*8*−*10*). The multiplicity of strategies for generation of the 3′-H-abstracting protein radical, which for all known RNRs is believed to be a cysteine thiyl radical, is the primary basis for the definition of three classes (I−III) of RNRs (*4*, *11*−*13*). The 5′-deoxyadenosyl radical, produced either by homolysis of the Co−C bond of 5′-deoxyadenosylcob(III)-alamin (*14*) (in class II) or by reductive cleavage of the C5′−S bond of *S*-adenosyl-L-methionine (in class III) (*15*, 16), is the ultimate source of the oxidizing equivalent for protein radical production in the class II and III RNRs. In class I RNRs, such as those found in aerobically growing *Escherichia coli* and in eukaryotes from *Saccharomyces cerevisiae* to *Homo sapiens*, activation of dioxygen at the carboxylate-bridged diiron(II/II) cluster harbored in the enzyme's R2 subunit introduces a stable tyrosyl free-radical into R2 by univalent oxidation of a buried tyrosine (Y122 in *E. coli* R2, which is the subject of this study) (*17*−*20*). This stoichiometric, autoactivation process yields the active R2 subunit, which functions catalytically in nucleotide reduction. Transient transfer of the oxidizing equivalent from the Y122 radical (Y122•) to a cysteine residue in the R1 subunit (C439 (*8*−*10*)) prepares R1 for the crucial 3′-H abstraction (*21*). Chemical steps involving additional cysteine residues in R1 (C225 and C462) then convert the 3′-centered substrate radical to the corresponding 3′ product radical, with formation of a C225−C462 disulfide (*8*, *22*, *23*). The 3′-H is then returned to complete the transformation to product, and subsequent reverse radical transfer regenerates the Y122• in R2 and reduced (nonradical) C439 in R1 (*8*, *21*).

The mechanistic pathway for Y122• formation has been mapped in some detail, beginning with the seminal studies in the early 1990s led by Stubbe (*24*−*30*). Addition of O_2 to the reactive form of the diiron(II/II) cluster, which is formed after acquisition of two Fe(II) ions and a conformational change by the R2 protein, leads to accumulation of a state containing the diiron(III/IV) cluster, **X** (*24*−*26*, *31*), and a cation radical harbored on the near-surface residue, W48 (*28*, *32*). In the presence of a one-electron reductant (e.g., ascorbate, thiols, $Fe(II)_{aq}$), the $W48^{+\bullet}$ is rapidly reduced (*25*, *28*, *32*). Under these conditions, the Y122• and (μ-oxo)-diiron(III/III) cluster of the native protein are generated in the last and slowest step of the reaction when cluster **X** oxidizes Y122 (*25*, *27*). The identities of precursors to the **X**−$W48^{+\bullet}$ state having both oxidizing equivalents of the initial diiron(II)−O_2 complex still localized on the diiron

† This work was supported by a grant from the Public Health Services (GM55365).

* To whom correspondence should be addressed. Tel, (814) 863-5707; fax, (814) 863-7024; e-mail, jmb21@psu.edu.

[1] Abbreviations: RNR, ribonucleotide reductase; R2, R2 subunit of *Escherichia coli* RNR; Y122•, tyrosyl radical in R2; $W48^{+\bullet}$, tryptophan 48 cation radical; wt, wild-type; IPTG, isopropy-β-D-thiogalactopyranoside; PMSF, phenylmethylsulfonyl fluoride; Tris, tris-[hydroxymethyl]-aminomethane; EPPS, (*N*-[2-hydroxyethyl]piperazine-*N*′-[3-propane-sulfonic acid]; HEPES, 4-(2-hydroxyethyl)-1-piperazineethanesulfonic acid; PCR, polymerase chain reaction; bp, base pairs; buffer A, 25 mM EPPS, pH 8.2; ($A_{411} - (A_{405} + A_{417})/2$), peak height proportional to the concentration of Y122•; ϵ_{280}, molar absorption coefficients at 280 nm; k_{obs}, observed apparent first-order rate constant.

10.1021/bi060325d CCC: $33.50
Published on Web 06/29/2006

cluster have not been definitively established, but Stubbe and co-workers presented evidence that a μ−(1,2-peroxo)diiron-(III/III) complex is among them (*30*). Indeed, our recent studies support this proposal (*33*) and further suggest (1) that the μ−1,2-peroxide isomerizes rapidly to a state, designated **L**, with two structurally distinct peroxodiiron(III/III) complexes in rapid equilibrium, and (2) that this state is the immediate precursor to the **X**−W48$^{+\bullet}$ state (*34*).

The mechanism of the radical-transfer step that initiates nucleotide reduction is less well-understood.[2] The structure of the holoenzyme (R1·R2) complex has not been been reported, but in silico docking of structures of the individual subunits of the *E. coli* enzyme at their most likely interface would position C439 in R1 >35 Å from the buried Y122· in R2 (*4*, *10*, *48*), much too great a distance for the reaction to occur at the required rate ($\geq 10^0-10^1$ s^{-1}, the rate constant reported both for steady-state and single turnover) via a single-step, electron-tunneling mechanism (*21*). A network of hydrogen-bonded, mostly aromatic amino acid residues that extends from Y122· in R2 toward the putative subunit interface and from the interface toward C439 in the active site of R1 (Y122·−W48−Y356- -Y731−Y730−C439, where the double hyphen marks the R2- -R1 interface) is thought to mediate radical transfer by a multistep-tunneling ("radical-hopping") mechanism that may also involve coupled proton transfer (*21*). In the simplest version of such a mechanism, the first and second steps would be oxidation of W48 by Y122· and reduction of the resulting W48$^{+\bullet}$ by Y356, and the last and penultimate steps of the reverse radical transfer would be the reverse of these two steps, respectively. Thus, according to this scenario, the W48$^{+\bullet}$ is likely to be an intermediate in intersubunit radical transfer, as it is in O_2 activation and Y122· formation.

The accumulation of W48$^{+\bullet}$ to more than 0.6 equiv during O_2 activation by the reduced *E. coli* R2 protein under appropriate reaction conditions[3] (*32*) creates the opportunity to study mechanisms of electron transfer to this likely intermediate in R1−R2 radical transfer. Earlier work showed that, in addition to its reduction by Fe(II)$_{aq}$ or other agents, the W48$^{+\bullet}$ can also be reduced by Y122 (*28*, *32*). This step, which would be analogous to the last step in the reverse (R1 → R2) radical transfer occurring in each turnover, is ~10-fold faster than oxidation of Y122 by **X** and thus gives rise to a fast phase of Y122· production specifically when the reaction is carried out in the absence of an exogenous W48$^{+\bullet}$ reductant. In this study, we have characterized the kinetics of decay of the W48$^{+\bullet}$ in the absence of reductants in the reactions of the wild-type R2 protein and its Y122F, Y356F, and Y122F/Y356 variants, thereby dissecting the decay process into constituent pathways. Our purpose was to understand more thoroughly electron/radical flow in R2 and to provide the foundation for possible transfer into R1 of oxidizing equivalents generated in R2 by O_2 activation. The latter notion, originally suggested by the work of Cooperman and co-workers showing that the mouse R2−Y177F variant (Y177 is the radical-harboring tyrosine in mouse R2, equivalent to Y122 in the *E. coli* protein) retains a low level of RNR activity in the presence of R1 (*49*), has become particularly relevant with the recent report that R2 subunits in certain hyperthermophilic archaea and pathogenic eubacteria lack the radical tyrosine (*50*, *51*) and the hypothesis that these RNRs may function by using an intermediate in O_2 activation to generate the R1 radical (*51*, *52*). Here, we show that the presence of Mg^{2+} at concentrations similar to that used in RNR activity assays brings Y356 into a rapid radical-transfer equilibrium with the W48$^{+\bullet}$, leading to a very rapid phase of Y· formation (Y356·) and an efficient pathway for decay of the W48$^{+\bullet}$.

MATERIALS AND METHODS

Materials. Culture media components (yeast extract and tryptone) were purchased from Marcor Development Corporation (Hackensack, NJ). Isopropy-β-D-thiogalactopyranoside (IPTG) was purchased from Biosynth International (Naperville, IL). Ampicillin was purchased from IBI (Shelton, CT). Phenylmethylsulfonyl fluoride (PMSF), streptomycin sulfate, *tris*-[hydroxymethyl]-aminomethane (Tris), 1,10-phenanthroline, and (*N*-[2-hydroxyethyl]piperazine-*N*′-[3-propane-sulfonic acid]) (EPPS) were purchased from Sigma (St. Louis, MO). Glycerol, ammonium sulfate, sodium chloride, sodium sulfate, and potassium chloride were purchased from EM Science (Gibbstown, NJ). Calcium chloride was purchased from Fisher Scientific (Fair Lawn, NJ). Magnesium sulfate and magnesium chloride were purchased from J. T. Baker Chemical Co. (Phillipsburg, NJ). Enzyme grade 4-(2-hydroxyethyl)-1-piperazineethanesulfonic acid (HEPES) was purchased from FisherBiotech (Pittsburgh, PA). Oligonucleotide primers were purchased from Invitrogen (Frederick, MD). Reagents for the polymerase chain reaction (PCR) and restriction enzymes were purchased from New England Biolabs (Beverly, MA). T4 DNA ligase was purchased from Roche (Indianapolis, IN). BL21(DE3) and pET vectors were purchased from Novagen (Madison, WI).

Preparation of Expression Vectors for R2-Y122F, R2-Y356F, and R2-Y122F/Y356F. Overexpression of R2-Y122F was directed by the plasmid pR2-Y122F(*Hind*III). This plasmid was prepared from two previously described plasmids: the smaller fragment (containing codons 52−210) from digestion of pR2-W48F/Y122F (*34*) with *Aat*II and *Hind*III was ligated with the larger fragment from digestion of pR2wt-*Hind*III (*53*) with the same enzymes. The codon change giving the Y356F substitution was introduced into the *nrdB* gene (encoding R2) by using PCR. The 3′-most third of the gene was amplified in two fragments by using four primers and pR2wt-*Hind*III (*53*), as template. Primers 1 (5′-CGT TTC TAC GT**A AGC TT**T GCT TGT TCC-3′)

[2] In fact, radical transfer has never actually been directly demonstrated. Indirect evidence that it occurs is, nevertheless, overwhelming and consists of the demonstrations that (1) R2 proteins lacking the tyrosyl radical (the "met", apo, and reduced forms of wild-type R2's and the Y → F variants) are inactive (*17*, *19*), (2) variants of R2 and R1 with residues in the putative radical-transfer pathway replaced have no or drastically diminished activities (*8*, *9*, *35*−*39*), (3) one of these variants (the Y370W variant of mouse R2) causes loss of the tyrosyl radical (Y177·) in a process that is dependent on substrate and R1 (*39*), (4) the C225S and E441Q variants of *E. coli* R1 mediate loss of the Y122· and the latter formation of new substrate and R1 radicals (in sequence) (*8*, *22*, *23*, *40*−*42*), and (5) substrates with radical-trapping functional groups (e.g., 2′-deoxy-2′-azido-nucleoside diphosphates and 2′-deoxy-2′-fluoromethylene-nucleoside diphosphates) cause decay of the tyrosyl radical and formation of new substrate- or R1-derived radicals (*43*−*47*).

[3] These conditions consist of an absence of reductants and an Fe(II)/R2 ratio, 2.7−3.0 equiv, that balances the opposing requirements for a filled diiron site (to give rapid O_2 activation) and only low levels of unbound Fe(II) (to prevent the rapid reduction of the W48$^{+\bullet}$ that occurs if [Fe(II)$_{aq}$] is present) (*32*).

Scheme 1: Pathways for Decay of the $W48^{+\bullet}$ Intermediate in Oxygen Activation by *E. coli* R2

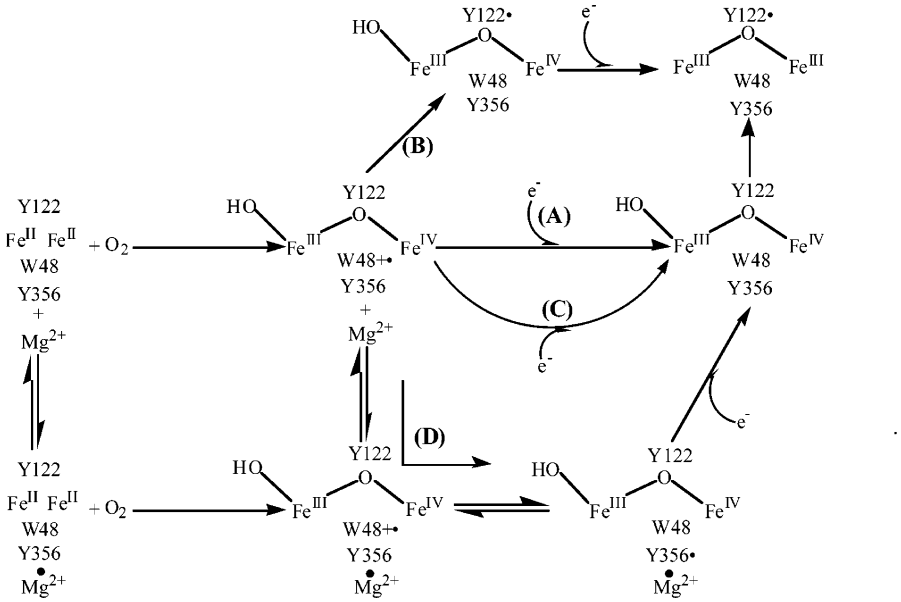

and 2 (5′-GAC CAG **AAA** AGA GCT CAC TTC CAC TTC C-3′) were used to amplify a 456 base-pair (bp) fragment of pR2wt-*Hind*III. Primer 1 anneals ~620 bp 3′ of the start of *nrdB* and contains the unique *HindIII* restriction site (in boldface type) previously introduced at codon V210 of *nrdB* (*53*). Primer 2 introduces both a translationally silent substitution that creates a unique *SacI* restriction site (underlined) at codon 354 of *nrdB* for internal ligation of the two fragments and the desired substitution at codon Y356 (TAT to TTT, complement of boldface triplet). A 1429 bp fragment of pR2wt-*Hind*III was amplified by using primers 3 (5′-GTG GAA GTG AGC TCT **TTT** CTG GTC-3′) and 4 (5′-CGC AAC GTT GTT GCC ATT G**CT GCA G**GC-3′). Primer 3 introduces the aforementioned *SacI* restriction site (underlined) and the desired substitution at codon Y356 (boldface triplet), and primer 4 contains the unique *PstI* site (in boldface type) 3′ of the *nrdB* gene for ligation with pR2wt-*Hind*III. The 456 bp PCR fragment was digested with *HindIII* and *SacI*, the 1429 bp PCR fragment was digested with *SacI* and *PstI*, and the vector pR2wt-*Hind*III was digested with *HindIII* and *PstI*. The fragments were joined in a three-piece ligation reaction to give the expression vector pR2-Y356F.

The overexpression vector for R2-Y122F/Y356F was prepared from pR2-Y122F and pR2−Y356F. The 532 bp *HindIII-XhoI* restriction fragment of pR2-Y356F was ligated with the large (vector) fragment from restriction of pR2-Y122F with the same enzymes to yield pR2-Y122F/Y356F.

The sequence of the coding region of each plasmid construct was verified to ensure that no undesired mutations had been introduced. DNA sequences were determined by the Nucleic Acid Facility of the Pennsylvania State University Biotechnology Institute.

Overexpression and Purification of R2-wt, R2-Y122F, R2-Y356F, and R2-Y122F/Y356F. Procedures used to overexpress and purify the proteins in the apo form have been described previously (*54*). Protein concentrations were determined spectrophotometrically by using molar absorption coefficients at 280 nm (ϵ_{280}) calculated according to the method of Gill and von Hippel (*55*). The ϵ_{280} values are 118 mM^{-1} cm^{-1} for apo R2-Y122F and apo R2-Y356F and 115 mM^{-1} cm^{-1} for apo R2-Y122F/Y356F.

Stopped-Flow Absorption Spectrophotometry. Stopped-flow absorption experiments were carried out with an Applied Photophysics SX.18MV stopped-flow apparatus (path length of 1 cm and dead-time of 1.3 ms) equipped with a diode array detector and housed in an anoxic chamber (MBraun). Solutions of apo R2 proteins in 25 mM EPPS, pH 8.2 (buffer A), were rendered free of oxygen on a vacuum/gas manifold and then mixed with Fe(II) in the anoxic chamber, as previously described (*54*). Oxygen-free Fe(II)−R2 samples were mixed with oxygen-saturated salt solutions prepared in buffer A. The temperature was maintained at 11 °C with a Lauda K-4/R circulating water bath. Kinetic traces shown represent averages of at least three trials. Specifics of reaction conditions are given in the figure legends.

RESULTS AND DISCUSSION

The kinetic and mechanistic complexity of the R2 reaction makes it advantageous to have an overview of the mechanism as a framework for subsequent interpretation of the data. Previous results and those presented below are consistent with the following mechanism. Decay of the $W48^{+\bullet}$ is complex and consists of at least four constituent pathways (Scheme 1). Fast reduction of the $W48^{+\bullet}$ by thiols, ascorbate, or $Fe(II)_{aq}$ when one of these is present (pathway A) and somewhat slower reduction by Y122 when reductants are absent (pathway B) have previously been demonstrated (*28*, *32*).[4] A third pathway (C) explains the eventual decay of the $W48^{+\bullet}$ even when reductants and both relevant tyrosines (Y122 and Y356) are absent (i.e., in R2-Y122F/Y356F). Associated with this pathway, a transient $Y^{\bullet}$ is produced from one of the 14 remaining (irrelevant) tyrosines. Thus, transient Y radicals are observed in the reactions of both R2-Y122F

[4] The cited study was conducted at 5 °C. The presence of the Y122F substitution introduces kinetic complexity in the O_2 addition step below 10 °C. This study has been carried out at 11 °C to obviate this additional complexity.

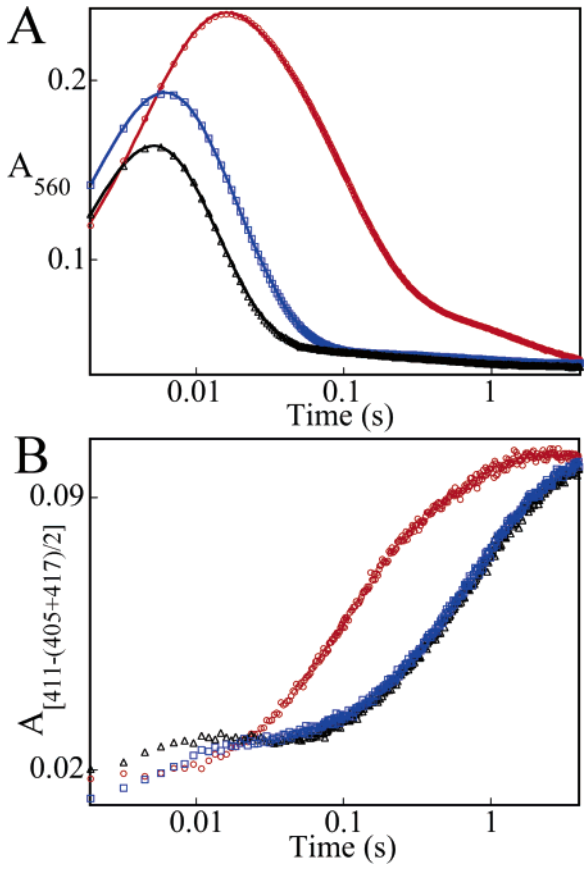

FIGURE 1: Effect of increasing [$MgCl_2$] on the kinetics of (A) the transient $W48^{+\bullet}$ monitored at 560 nm and (B) Y· monitored by the 411-nm peak height [$A_{411} - (A_{405} + A_{417})/2$] in the reaction of Fe(II)−R2−wt with O_2. A solution of O_2-free Fe(II)−R2−wt in buffer A was mixed at 11 °C with an equal volume of O_2-saturated buffer A containing different concentrations of $MgCl_2$. The final concentration of R2 after mixing was 0.1 mM (Fe(II)/R2 = 2.7). The final concentrations of $MgCl_2$ after mixing were 0 mM (red circles), 21 mM (blue squares), and 210 mM (black triangles). The solid lines in panel A are fits, as described in the text.

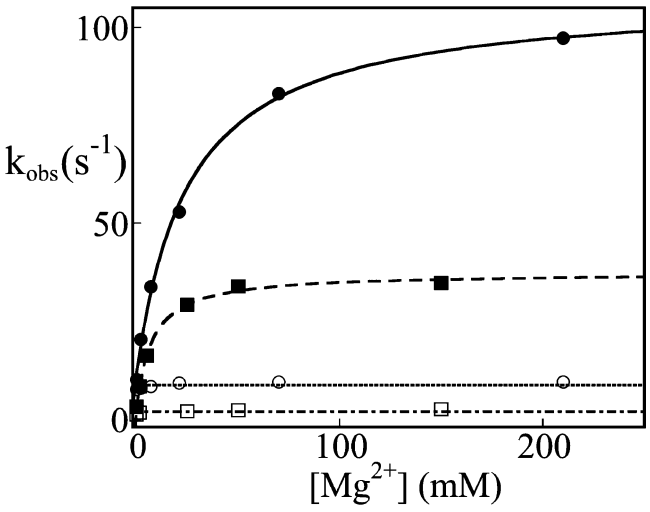

FIGURE 2: Dependence of the observed rate constant of $W48^{+\bullet}$ decay on [$MgCl_2$] in the reactions of R2−wt (filled circles and solid line), R2-Y122F (filled squares and dashed line), R2-Y356F (open circles and dotted line), and R2-Y122F/Y356F (open squares and dotted-dashed line). The solid and dashed lines are fits of the equation for a hyperbola to the data and correspond to $K_{0.5}$ values of 26 ± 3 mM and 8 ± 1 mM and k_{max} values of 108 ± 4 s^{-1} and 37 ± 2 s^{-1} for R2−wt and R2-Y122F, respectively. The dotted and dotted-dashed lines are lines of zero slope to indicate the near absence of an effect of Mg^{2+} on the reaction of proteins lacking Y356. The experimental conditions are described in legends to Figure 1 (R2−wt), Figure 3 (R2−Y356F), Figure 4 (R2−Y122F), and Figure 5 (R2−Y122F/Y356F).

and R2-Y122F/Y356F, but only for R2-Y122F are the kinetics of the transient Y· sensitive to variation in [Mg^{2+}] (as described in detail below). Because the quantity of transient Y· in the reaction of the double variant appears to be insufficient to account for all the $W48^{+\bullet}$ that decays (based on the known molar absorptivity of the $W48^{+\bullet}$ (*28*, *32*) and reasonable estimates for that of the Y·), this pathway is probably decomposable into additional components, of which one (or more) generates a Y· and one (or more) does not. Because all of its constituent processes are relatively slow, this pathway competes ineffectively with other pathways in all reactions but that of the double variant and is not considered in detail. Pathways A−C are all independent of both Mg^{2+} and Y356. The fourth and, for the purposes of this study, most interesting pathway (D) results from a Mg^{2+}-dependent interaction of the $W48^{+\bullet}$ with Y356. Kinetic manifestations of it and evidence that it results from a Mg^{2+}-dependent radical-transfer equilibrium between W48 and Y356 will now be summarized.

Consistent with previous studies carried out at a reaction temperature of 5 °C (*32*), mixing of the Fe(II)−R2−wt complex at 11 °C with O_2-saturated buffer results in the rapid development of the broad 560-nm absorption band of the $W48^{+\bullet}$, followed by decay of this feature and formation of the sharp 411-nm feature characteristic of tyrosyl radical (not shown). Inclusion of Mg^{2+} in the O_2-saturated buffer solution markedly affects the kinetics (Figure 1). Previous studies (*32*) have shown that the A_{560} traces (Figure 1A) have three kinetic phases: a rapid rise phase, which corresponds to formation of the **X**−$W48^{+\bullet}$ state; a fast decay phase, which corresponds to the sum of pathways A−C in Scheme 1; and a slower decay phase, which corresponds to reduction of **X** either by Y122 or an unknown exogenous source (two steps leading to native R2 in top right corner of Scheme 1). The A_{560} traces were therefore fit by the equation for three exponential phases in order to resolve and quantify the contribution of pathway D in Scheme 1 to decay of $W48^{+\bullet}$. The fits reveal that Mg^{2+} affects the effective first-order rate constant for formation of $W48^{+\bullet}$ to only a minor extent (<2-fold faster at the highest [Mg^{2+}]). By contrast, increasing [Mg^{2+}] markedly accelerates decay of $W48^{+\bullet}$ (Figure 1A). The observed first-order rate constant for decay increases hyperbolically with [Mg^{2+}] (Figure 2, filled circles and solid line), "saturating" at a value of 108 ± 3 s^{-1}, 9 times the k_{obs} in the absence of Mg^{2+}. The effect of Mg^{2+} on the kinetics of Y· formation (as assessed by the intensity of the diagnostic sharp ~411 nm peak characteristic of Y radicals) is complex (Figure 1B). At high [Mg^{2+}], a minor phase of very rapid Y· formation is observed and is nearly coincident with development of the 560-nm feature of the $W48^{+\bullet}$. This rapid phase is followed by overall *slower* formation of stable Y· (presumably Y122·). The overall slowing of Y122· production by increasing [Mg^{2+}] is attributable to engagement of a more efficient pathway for decay of $W48^{+\bullet}$ (pathway D). When the Mg^{2+}-dependent pathway is *not* engaged, $W48^{+\bullet}$ decays primarily by oxidation of Y122 (pathway B). This step is faster than oxidation of Y122 by **X**, which occurs following decay of $W48^{+\bullet}$ by

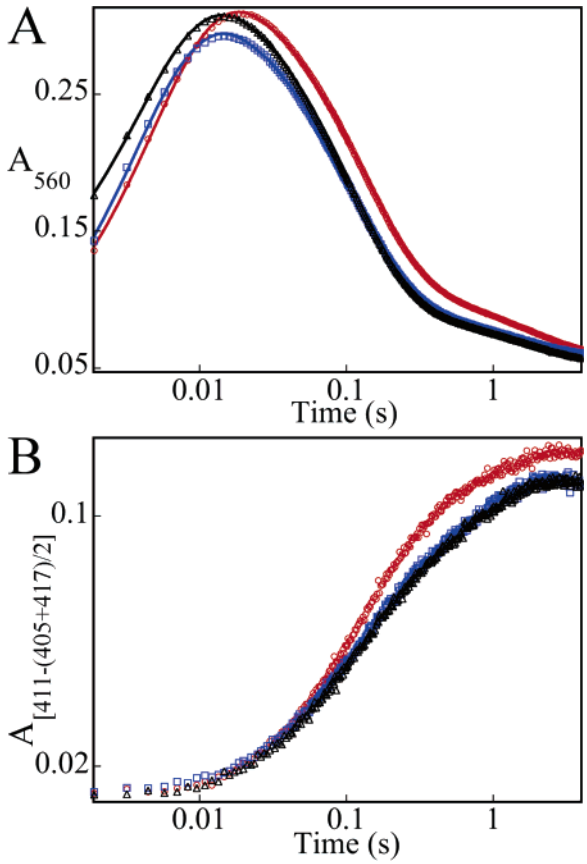

FIGURE 3: Effect of increasing [$MgCl_2$] on the kinetics of (A) the transient $W48^{+\bullet}$ monitored at 560 nm and (B) Y· monitored by the 411-nm peak height [$A_{411} - (A_{405} + A_{417})/2$] in the reaction of Fe(II)−R2−Y356F with O_2. A solution of O_2-free Fe(II)−R2−Y356F in buffer A was mixed at 11 °C with an equal volume of O_2-saturated buffer A containing different concentrations of $MgCl_2$. The final concentration of the protein after mixing was 0.1 mM (Fe(II)/R2 = 2.7). The final concentrations of $MgCl_2$ after mixing were 0 mM (red circles), 21 mM (blue squares), and 210 mM (black triangles). The solid lines in panel A are fits, as described in the text.

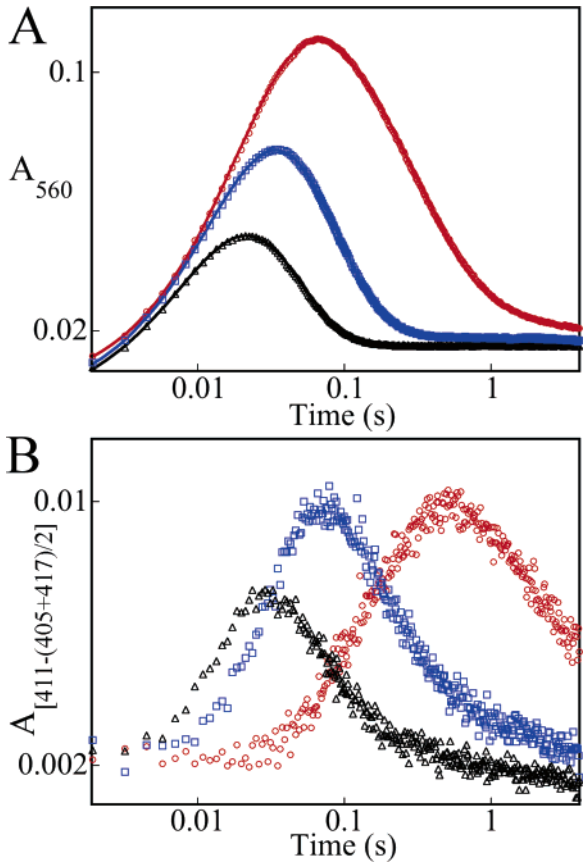

FIGURE 4: Effect of increasing [$MgCl_2$] on the kinetics of (A) the transient $W48^{+\bullet}$ monitored at 560 nm and (B) Y· monitored by the 411-nm peak height [$A_{411} - (A_{405} + A_{417})/2$] in the reaction of Fe(II)−R2−Y122F with O_2. A solution of O_2-free Fe(II)−R2−Y122F in buffer A was mixed at 11 °C with an equal volume of O_2-saturated buffer A containing different concentrations of $MgCl_2$. The final concentration of the protein after mixing was 0.06 mM (Fe(II)/R2 = 2.7). The final concentrations of $MgCl_2$ after mixing were 0 mM (red circles), 5 mM (blue squares), and 50 mM (black triangles). The solid lines in panel A are fits, as described in the text.

pathway A, C, or D. Thus, the overall slowing of Y122· production when pathway D is engaged by high [Mg^{2+}] is similar to that previously reported for inclusion of a reductant to quench the $W48^{+\bullet}$ via pathway A.

The results of identical experiments on the reaction of R2-Y356F (Figure 3) demonstrate that the pronounced effects of Mg^{2+} on $W48^{+\bullet}$ decay and Y· formation depend on the presence of Y356. Increasing [Mg^{2+}] does not accelerate decay of the 560-nm absorption feature in this variant (or does so to a much lesser extent) (Figure 3A and Figure 2, open circles and dotted line). In addition, Mg^{2+} barely affects the kinetics of Y122· formation (Figure 3B). Notably, the very fast phase of Y· formation is absent in the variant, implying that the fast phase of Y· formation in the reaction of R2−wt at high [Mg^{2+}] arises from Y356· formation. Evidence for oxidation of Y356 upon O_2 activation by R2-Y122F was previously presented (*24*, 56), but the linkage of this process to the presence of cations was not explored. The fact that Y356· formation is, at high [Mg^{2+}], roughly coincident with $W48^{+\bullet}$ formation suggests that the two radicals are in equilibrium, and the fact that the fast phase has a much smaller amplitude than that of subsequent Y122· formation implies that the Y356· is disfavored in its equilibrium with $W48^{+\bullet}$.

The effects of Mg^{2+} on the kinetics of the reactions of R2-Y122F and R2-Y122F/Y356F are consistent with the above interpretation. $W48^{+\bullet}$ decay is slower overall in these variants, as a result of the absence of the pathway for its reduction by Y122 (pathway B). In addition, and as expected, no stable Y· is produced. In the single variant, increasing [Mg^{2+}] is associated with increasingly rapid decay of the $W48^{+\bullet}$ (Figure 4A), as in the reaction of R2−wt. The dependence on [Mg^{2+}] is again hyperbolic (Figure 2, filled squares and dashed line), in this case reaching a limiting value for k_{obs} of 37 ± 2 s^{-1}. This value represents a 12-fold acceleration relative to decay in the absence of Mg^{2+}. The $K_{0.5}$ is 8 ± 1 mM, ~3-fold less than that for R2−wt. Associated with the faster decay of $W48^{+\bullet}$, formation and decay of a transient Y· become much faster at high [Mg^{2+}] (Figure 4B). The peak of [Y·] shifts to earlier time by ~17-fold, and the formation phase becomes roughly coincident with formation of the $W48^{+\bullet}$, as in the R2−wt reaction. None of these effects occur in R2-Y122F/Y356F: $W48^{+\bullet}$ is accelerated to a minor extent (Figure 5A and Figure 2, open squares and dotted-dashed line), and the kinetics of transient Y· are hardly affected (Figure 5B) by increasing [Mg^{2+}]. The fact that a transient Y· is observed at all in the double variant implies that one or more of the 14 tyrosines

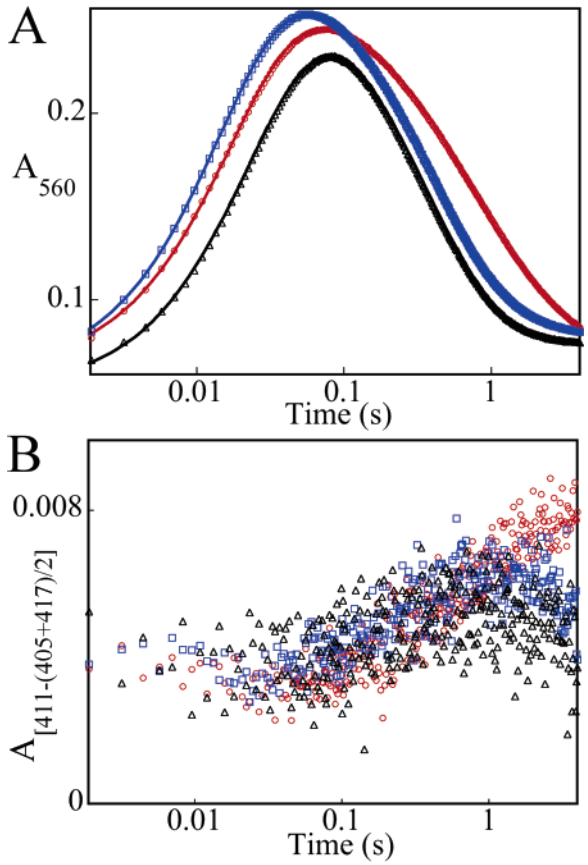

FIGURE 5: Effect of increasing [$MgCl_2$] on the kinetics of (A) the transient $W48^{+\bullet}$ monitored at 560 nm and (B) Y· monitored by the 411-nm peak height [$A_{411} - (A_{405} + A_{417})/2$] in the reaction of Fe(II)−R2−Y122F/Y356F with O_2. A solution of O_2-free Fe(II)−R2−Y122F/Y356F in buffer A was mixed at 11 °C with an equal volume of O_2-saturated buffer A containing different concentrations of $MgCl_2$. The final concentration of the protein after mixing was 0.09 mM (Fe(II)/R2 = 2.7). The final concentrations of $MgCl_2$ after mixing were 0 mM (red circles), 21 mM (blue squares), and 210 mM (black triangles). The solid lines in panel A are fits, as described in the text.

other than Y122 and Y356 can be oxidized during decay of $W48^{+\bullet}$. The important point is that this process is very slow and unaffected by Mg^{2+}. In contrast, the transient Y· in the presence of both Y356 and high [Mg^{2+}] develops rapidly, on the same time scale as O_2 addition.

Variation of the anion and cation in the reaction of R2-Y122F was undertaken to verify that the latter is the relevant mediator of the W48−Y356 radical-transfer equilibrium (Figure 6). Chloride and sulfate salts of Mg^{2+} and Ca^{2+} have equivalent effects and concentration dependencies (filled symbols). The identity of the anion is unimportant. Salts of monovalent cations also mediate the effect, but much higher concentrations (hundreds of millimolar) are required (open symbols). Again, the identity of the anion is unimportant. These data establish that the cation is the mediator and that divalent cations are ~33-fold more efficient as mediators than monovalent cations (comparing the limiting slopes of plots of k_{obs} versus [M^{n+}]). Notably, this difference is greater than the 3-fold difference between monovalent and divalent cations that would be expected if the effect were due merely to increasing ionic strength.

The kinetic data for the reactions of the four R2 proteins thus reveal a cation-dependent radical-transfer equilibrium

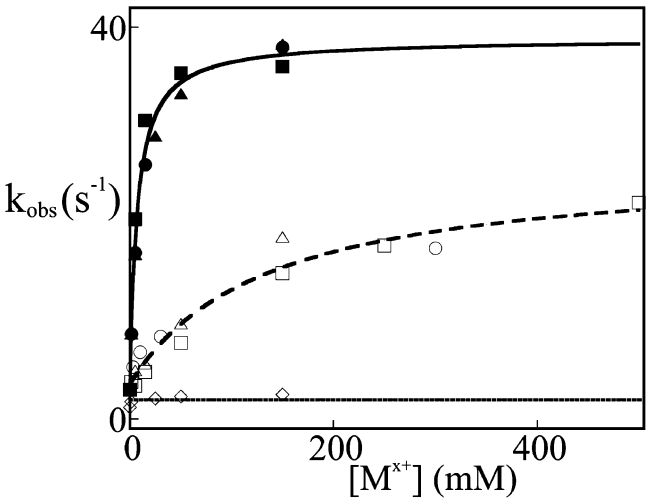

FIGURE 6: Titration of the effects of different salts on the observed rate constant for decay of $W48^{+\bullet}$ in the reaction of R2-Y122F. A solution of O_2-free Fe(II)−R2−Y122F complex (0.1−0.2 mM; Fe(II)/R2 = 2.7) was mixed at 11 °C with an equal volume of O_2-saturated buffer containing different concentrations of Na_2SO_4 (open squares), NaCl (open circles), KCl (open triangles), $MgCl_2$ (closed squares), $CaCl_2$ (closed circles), or $MgSO_4$ (closed triangles) in the stopped-flow apparatus. The rate constants for decay of $W48^{+\bullet}$ were obtained from the fits of the kinetic traces of $W48^{+\bullet}$ (as described in the text). The solid and dashed lines are fits of the equation for a hyperbola to the data for the divalent cations and monovalent cations, respectively, and the values at half-maximal enhancement of $W48^{+\bullet}$ decay ($K_{0.5}$) are calculated to be 8.6 ± 0.5 mM for the divalent cations and 210 ± 27 mM for the monovalent cations. As a control, a solution of O_2-free Fe(II)−R2−Y122F/Y356F complex (0.13 mM; Fe(II)/R2 = 2.7) was mixed at 11 °C with an equal volume of O_2-saturated buffer containing different concentrations of $MgSO_4$ (open diamonds).

between W48 and Y356. The mechanism and functional significance of the phenomenon remain open questions. Although there are multiple possible mechanisms, we consider the simplest and most probable to be binding of the cation in the vicinity of Y356. Cation binding could influence the relative potentials of W48 and Y356. Alternatively (or in addition), simultaneous coordination of one or more side chain both in the C-terminus and in the main domain of the protein could "tether" the flexible C-terminus to the protein to decrease the effective distance between W48 and Y356. Indeed, X-ray crystal structures of R2 reveal two carboxylate residues within 8 Å of W48 (*20*, *57*, *58*). E51 and E52 would be excellent candidates for C-terminus-tethering Mg^{2+} ligands. In fact, E52 is conserved among R2 sequences. In addition, the C-terminus is rich in residues that could serve as Mg^{2+} ligands (E and D residues and perhaps even Y356 itself). Intriguingly, C-terminal carboxylate residue E350 is also conserved (one of a few residues in the C-terminus) and has been subjected to site-directed mutagenesis (*35*). The E350A variant was found to be *inactive in nucleotide reduction*, even though its affinity for R1 is normal (*35*). To our knowledge, the inactivity of this variant has not yet been explained. It raises the possibility that E350 may function as a Mg^{2+} ligand to mediate communication between W48 and Y356 as part of the radical-transfer steps that initiate and culminate nucleotide reduction. It is noteworthy that the standard RNR assay includes 15 mM Mg^{2+}, similar to the $K_{0.5}$ value determined for R2−wt in our experiments and greater than that for R2-Y122F. Moreover,

binding of Mg^{2+} and R1 by R2 could be synergistic, reducing the concentration of Mg^{2+} needed to mediate communication between Y356 and W48 in the R1·R2 complex. We are not aware of any report in which the dependence of turnover on [Mg^{2+}] was documented, and so our suggestion that one role of Mg^{2+} [in addition to binding of nucleotides and its reported requirement for maintenance of the functional R1 homodimer (*59*)] could be to mediate intersubunit radical transfer must be considered as speculative. Mutagenesis experiments and activity measurements to test the intriguing possibility are in progress.

REFERENCES

1. Thelander, L., and Reichard, P. (1979) Reduction of ribonucleotides, *Annu. Rev. Biochem. 48*, 133−158.
2. Stubbe, J. (1990) Ribonucleotide reductases, *Adv. Enzymol. Relat. Areas Mol. Biol. 63*, 349−419.
3. Jordan, A., and Reichard, P. (1998) Ribonucleotide reductases, *Annu. Rev. Biochem. 67*, 71−98.
4. Eklund, H., Uhlin, U., Farnegardh, M., Logan, D. T., and Nordlund, P. (2001) Structure and function of the radical enzyme ribonucleotide reductase, *Prog. Biophys. Mol. Biol. 77*, 177−268.
5. Stubbe, J., and Ackles, D. (1980) On the mechanism of ribonucleotide diphosphate reductase from *Escherichia coli*, *J. Biol. Chem. 255*, 8027−8030.
6. Stubbe, J., Ackles, D., Segal, R., and Blakley, R. L. (1981) On the mechanism of ribonucleoside triphosphate reductase from *Lactobacillus leichmannii*. Evidence for 3′ carbon−hydrogen bond cleavage, *J. Biol. Chem. 256*, 4843−4846.
7. Stubbe, J., Ator, M., and Krenitsky, T. (1983) Mechanism of ribonucleoside diphosphate reductase from *Escherichia coli*. Evidence for 3′-C-H bond cleavage, *J. Biol. Chem. 258*, 1625−1631.
8. Mao, S. S., Holler, T. P., Yu, G. X., Bollinger, J. M., Jr., Booker, S., Johnston, M. I., and Stubbe, J. (1992) A model for the role of multiple cysteine residues involved in ribonucleotide reduction: amazing and still confusing, *Biochemistry 31*, 9733−9743.
9. Mao, S. S., Yu, G. X., Chalfoun, D., and Stubbe, J. (1992) Characterization of C439SR1, a mutant of *Escherichia coli* ribonucleotide diphosphate reductase: evidence that C439 is a residue essential for nucleotide reduction and C439SR1 is a protein possessing novel thioredoxin-like activity, *Biochemistry 31*, 9752−9759.
10. Uhlin, U., and Eklund, H. (1994) Structure of ribonucleotide reductase protein R1, *Nature 370*, 533−539.
11. Reichard, P. (1993) From RNA to DNA, why so many ribonucleotide reductases?, *Science 260*, 1773−1776.
12. Reichard, P. (1997) The evolution of ribonucleotide reduction, *Trends Biochem. Sci. 22*, 81−85.
13. Stubbe, J., and van der Donk, W. A. (1998) Protein radicals in enzyme catalysis, *Chem. Rev. 98*, 705−762.
14. Booker, S., Licht, S., Broderick, J., and Stubbe, J. (1994) Coenzyme B12-dependent ribonucleotide reductase: evidence for the participation of five cysteine residues in ribonucleotide reduction, *Biochemistry 33*, 12676−12685.
15. Ollagnier, S., Mulliez, E., Gaillard, J., Eliasson, R., Fontecave, M., and Reichard, P. (1996) The anaerobic *Escherichia coli* ribonucleotide reductase. Subunit structure and iron−sulfur center, *J. Biol. Chem. 271*, 9410−9416.
16. Ollagnier, S., Mulliez, E., Schmidt, P. P., Eliasson, R., Gaillard, J., Deronzier, C., Bergman, T., Gräslund, A., Reichard, P., and Fontecave, M. (1997) Activation of the anaerobic ribonucleotide reductase from *Escherichia coli*. The essential role of the iron−sulfur center for S-adenosylmethionine reduction, *J. Biol. Chem. 272*, 24216−24223.
17. Atkin, C. L., Thelander, L., and Reichard, P. (1973) Iron and free radical in ribonucleotide reductase. Exchange of iron and Mössbauer spectroscopy of the protein B2 subunit of the *Escherichia coli* enzyme, *J. Biol. Chem. 248*, 7464−7472.
18. Larsson, A., and Sjöberg, B.-M. (1986) Identification of the stable free radical tyrosine residue in ribonucleotide reductase, *EMBO J. 5*, 2037−2040.
19. Larsson, A., Karlsson, M., Sahlin, M., and Sjöberg, B.-M. (1988) Radical formation in the dimeric small subunit of ribonucleotide reductase requires only one tyrosine 122, *J. Biol. Chem. 263*, 17780−17784.
20. Nordlund, P., and Eklund, H. (1993) Structure and function of the *Escherichia coli* ribonucleotide reductase, *J. Mol. Biol. 232*, 123−164.
21. Stubbe, J., Nocera, D. G., Yee, C. S., and Chang, M. C. Y. (2003) Radical initiation in the class I ribonucleotide reductase: long-range proton-coupled electron transfer?, *Chem. Rev. 103*, 2167−2202.
22. Mao, S. S., Johnston, M. I., Bollinger, J. M., and Stubbe, J. (1989) Mechanism-based inhibition of a mutant *Escherichia coli* ribonucleotide reductase (cysteine-225 → serine) by its substrate CDP, *Proc. Natl. Acad. Sci. U.S.A. 86*, 1485−1489.
23. Mao, S. S., Holler, T. P., Bollinger, J. M., Jr., Yu, G.-X., Johnston, M. I., and Stubbe, J. (1992) Interaction of C225SR1 mutant subunit of ribonucleotide reductase with R2 and nucleoside diphosphates: tales of a suicidal enzyme, *Biochemistry 31*, 9744−9751.
24. Bollinger, J. M., Jr., Stubbe, J., Huynh, B. H., and Edmondson, D. E. (1991) Novel diferric radical intermediate responsible for tyrosyl radical formation in assembly of the cofactor of ribonucleotide reductase, *J. Am. Chem. Soc. 113*, 6289−6291.
25. Bollinger, J. M., Jr., Edmondson, D. E., Huynh, B. H., Filley, J., Norton, J. R., and Stubbe, J. (1991) Mechanism of assembly of the tyrosyl radical-dinuclear iron cluster cofactor of ribonucleotide reductase, *Science 253*, 292−298.
26. Ravi, N., Bollinger, J. M., Jr., Huynh, B. H., Edmondson, D. E., and Stubbe, J. (1994) Mechanism of assembly of the tyrosyl radical-diiron(III) cofactor of *E. coli* ribonucleotide reductase: 1. Mössbauer characterization of the diferric radical precursor, *J. Am. Chem. Soc. 116*, 8007−8014.
27. Bollinger, J. M., Jr., Tong, W. H., Ravi, N., Huynh, B. H., Edmondson, D. E., and Stubbe, J. (1994) Mechanism of assembly of the tyrosyl-diiron(III) cofactor of *E. coli* ribonucleotide reductase. 2. Kinetics of the excess Fe^{2+} reaction by optical, EPR, and Mössbauer spectroscopies, *J. Am. Chem.* Soc. *116*, 8015−8023.
28. Bollinger, J. M., Jr., Tong, W. H., Ravi, N., Huynh, B. H., Edmondson, D. E., and Stubbe, J. (1994) Mechanism of assembly of the tyrosyl radical-diiron(III) cofactor of *E. coli* ribonucleotide reductase. 3. Kinetics of the limiting Fe^{2+} reaction by optical, EPR, and Mössbauer spectroscopies, *J. Am.* Chem. *Soc. 116*, 8024−8032.
29. Bollinger, J. M., Jr., Tong, W. H., Ravi, N., Huynh, B. H., Edmondson, D. E., and Stubbe, J. (1995) Use of rapid kinetics methods to study the assembly of the diferric-tyrosyl radical cofactor of *E. coli* ribonucleotide reductase, *Methods Enzymol. 258*, 278−303.
30. Tong, W. H., Chen, S., Lloyd, S. G., Edmondson, D. E., Huynh, B. H., and Stubbe, J. (1996) Mechanism of assembly of the diferric cluster-tyrosyl radical cofactor of *Escherichia coli* ribonucleotide reductase from the diferrous form of the R2 subunit, *J. Am. Chem. Soc. 118*, 2107−2108.
31. Sturgeon, B. E., Burdi, D., Chen, S., Huynh, B. H., Edmondson, D. E., Stubbe, J., and Hoffman, B. M. (1996) Reconsideration of **X**, the diiron intermediate formed during cofactor assembly in *E. coli* ribonucleotide reductase, *J. Am. Chem. Soc. 118*, 7551−7557.
32. Baldwin, J., Krebs, C., Ley, B. A., Edmondson, D. E., Huynh, B. H., and Bollinger, J. M., Jr. (2000) Mechanism of rapid electron transfer during oxygen activation in the R2 subunit of *Escherichia coli* ribonucleotide reductase. 1. Evidence for a transient tryptophan radical, *J. Am. Chem. Soc. 122*, 12195−12206.
33. Bollinger, J. M., Jr., Krebs, C., Vicol, A., Chen, S., Ley, B. A., Edmondson, D. E., and Huynh, B. H. (1998) Engineering the diiron site of *Escherichia coli* ribonucleotide reductase protein R2 to accumulate an intermediate similar to H_{peroxo}, the putative peroxodiiron(III) complex from the methane monooxygenase catalytic cycle, *J. Am. Chem. Soc. 120*, 1094−1095.
34. Saleh, L., Krebs, C., Ley, B. A., Naik, S., Huynh, B. H., and Bollinger, J. M., Jr. (2004) Use of a chemical trigger for electron transfer to characterize a precursor to cluster **X** in assembly of the iron-radical cofactor of *Escherichia coli* ribonucleotide reductase, *Biochemistry 43*, 5953−5964.
35. Climent, I., Sjöberg, B.-M., and Huang, C. Y. (1992) Site-directed mutagenesis and deletion of the carboxyl terminus of *Escherichia coli* ribonucleotide reductase protein R2. Effects on catalytic activity and subunit interaction, *Biochemistry 31*, 4801−4807.
36. Rova, U., Goodtzova, K., Ingemarson, R., Behravan, G., Gräslund, A., and Thelander, L. (1995) Evidence by site-directed mutagen-

esis supports long-range electron transfer in mouse ribonucleotide reductase, *Biochemistry 34*, 4267−4275.
37. Ekberg, M., Sahlin, M., Eriksson, M., and Sjöberg, B.-M. (1996) Two conserved tyrosine residues in protein R1 participate in an intermolecular electron transfer in ribonucleotide reductase, *J. Biol. Chem. 271*, 20655−20659.
38. Ekberg, M., Pötsch, S., Sandin, E., Thunnissen, M., Nordlund, P., Sahlin, M., and Sjöberg, B.-M. (1998) Preserved catalytic activity in an engineered ribonucleotide reductase R2 protein with a non-physiological radical transfer pathway. The importance of hydrogen bond connections between the participating residues, *J. Biol. Chem. 273*, 21003−21008.
39. Rova, U., Adrait, A., Pötsch, S., Gräslund, A., and Thelander, L. (1999) Evidence by mutagenesis that Tyr(370) of the mouse ribonucleotide reductase R2 protein is the connecting link in the intersubunit radical transfer pathway, *J. Biol. Chem. 274*, 23746−23751.
40. Persson, A. L., Eriksson, M., Katterle, B., Pötsch, S., Sahlin, M., and Sjöberg, B.-M. (1997) A new mechanism-based radical intermediate in a mutant R1 protein affecting the catalytically essential Glu441 in *Escherichia coli* ribonucleotide reductase, *J. Biol. Chem. 272*, 31533−31541.
41. Persson, A. L., Sahlin, M., and Sjöberg, B.-M. (1998) Cysteinyl and substrate radical formation in active site mutant E441Q of *Escherichia coli* class I ribonucleotide reductase, *J. Biol. Chem. 273*, 31016−31020.
42. Lawrence, C. C., Bennati, M., Obias, H. V., Bar, G., Griffin, R. G., and Stubbe, J. (1999) High-field EPR detection of a disulfide radical anion in the reduction of cytidine 5′-diphosphate by the E441Q R1 mutant of *Escherichia coli* ribonucleotide reductase, *Proc. Natl. Acad. Sci. U.S.A. 96*, 8979−8984.
43. Ator, M., Salowe, S. P., Stubbe, J., Emptage, M. H., and Robins, M. J. (1984) 2′-Azido-2′-deoxynucleotide interaction with *E. coli* ribonucleotide reductase: generation of a new radical species, *J. Am. Chem. Soc. 106*, 1886−1887.
44. Salowe, S. P., Ator, M. A., and Stubbe, J. (1987) Products of the inactivation of ribonucleoside diphosphate reductase from *Escherichia coli* with 2′-azido-2′-deoxyuridine 5′-diphosphate, *Biochemistry 26*, 3408−3416.
45. Stubbe, J., Booker, S., Broderick, J., Mao, S. S., Ator, M., Harris, G., Ashley, G., Linn, A. E., and Yu, G. X. (1993) Ribonucleotide reductases: radical enzymes with suicidal tendencies, *Nucleic Acids Symp. Ser. 29*, 107.
46. van der Donk, W. A., Yu, G., Silva, D. J., Stubbe, J., McCarthy, J. R., Jarvi, E. T., Matthews, D. P., Resvick, R. J., and Wagner, E. (1996) Inactivation of ribonucleotide reductase by (*E*)-2′-fluoromethylene-2′-deoxycytidine 5′-diphosphate: a paradigm for nucleotide mechanism-based inhibitors, *Biochemistry 35*, 8381−8391.
47. Gerfen, G. J., van der Donk, W. A., Yu, G., McCarthy, J. R., Jarvi, E. T., Matthews, D. P., Farrar, C., Griffin, R. G., and Stubbe, J. (1998) Characterization of a substrate-derived radical detected during the inactivation of ribonucleotide reductase from *Escherichia coli* by 2′-fluoromethylene-2′-deoxycytidine 5′-diphosphate, *J. Am. Chem. Soc. 120*, 3823−3835.
48. Sahlin, M., and Sjöberg, B.-M. (2000) Ribonucleotide reductase. A virtual playground for electron-transfer reactions, *Subcell. Biochem. 35*, 405−443.
49. Henriksen, M. A., Cooperman, B. S., Salem, J. S., Li, L.-S., and Rubin, H. (1994) The stable tyrosyl radical in mouse ribonucleotide reductase is not essential for enzymic activity, *J. Am. Chem. Soc. 116*, 9773−9774.
50. Roshick, C., Iliffe-Lee, E. R., and McClarty, G. (2000) Cloning and characterization of ribonucleotide reductase from *Chlamydia trachomatis*, *J. Biol. Chem. 275*, 38111−38119.
51. Högbom, M., Stenmark, P., Voevodskaya, N., McClarty, G., Gräslund, A., and Nordlund, P. (2004) The radical site in Chlamydial ribonucleotide reductase defines a new R2 subclass, *Science 305*, 245−248.
52. Voevodskaya, N., Lendzian, F., and Gräslund, A. (2005) A stable Fe^{III}-Fe^{IV} replacement of tyrosyl radical in a class I ribonucleotide reductase, *Biochem. Biophys. Res. Commun. 330*, 1213−1216.
53. Moënne-Loccoz, P., Baldwin, J., Ley, B. A., Loehr, T. M., and Bollinger, J. M., Jr. (1998) O_2 activation by non-heme diiron proteins: identification of a symmetric μ-1,2-peroxide in a mutant of ribonucleotide reductase, *Biochemistry 37*, 14659−14663.
54. Parkin, S. E., Chen, S., Ley, B. A., Mangravite, L., Edmondson, D. E., Huynh, B. H., and Bollinger, J. M., Jr. (1998) Electron injection through a specific pathway determines the outcome of oxygen activation at the diiron cluster in the F208Y mutant of *Escherichia coli* ribonucleotide reductase protein R2, *Biochemistry 37*, 1124−1130.
55. Gill, S. C., and von Hippel, P. H. (1989) Calculation of protein extinction coefficients from amino acid sequence data, *Anal. Biochem. 182*, 319−326.
56. Sahlin, M., Lassmann, G., Pötsch, S., Sjöberg, B.-M., and Gräslund, A. (1995) Transient free radicals in iron/oxygen reconstitution of mutant protein R2 Y122F. Possible participants in electron-transfer chains in ribonucleotide reductase, *J. Biol. Chem. 270*, 12361−12372.
57. Nordlund, P., Sjöberg, B.-M., and Eklund, H. (1990) Three-dimensional structure of the free radical protein of ribonucleotide reductase, *Nature 345*, 593−598.
58. Högbom, M., Galander, M., Andersson, M., Kolberg, M., Hofbauer, W., Lassmann, G., Nordlund, P., and Lendzian, F. (2003) Displacement of the tyrosyl radical cofactor in ribonucleotide reductase obtained by single-crystal high-field EPR and 1.4-Å X-ray data, *Proc. Natl. Acad. Sci. U.S.A. 100*, 3209−3214.
59. Thelander, L. (1973) Physicochemical characterization of ribonucleoside diphosphate reductase from *Escherichia coli*, *J. Biol. Chem. 248*, 4591−4601.

BI060325D